Properties of aligned poly(L-lactic acid) electrospun fibers

Bin Mao,[1] Keifer Geers,[2] Sophia Hu,[3] Marlet Mancera,[4] Myra Sandoval,[4] Joshua Port,[1] Yazhe Zhu,[1] Peggy Cebe[1]

[1]Department of Physics and Astronomy, Center for Nanoscopic Physics, Tufts University, Medford, Massachusetts 02155
[2]Department of Biomedical Engineering, Texas A&M University, College Station, Texas 77843
[3]Department of Chemistry, University of Pennsylvania, Philadelphia, Pennsylvania 19104
[4]National Technical Institute for the Deaf, Rochester Institute of Technology, Rochester, New York 14623
Correspondence to: P. Cebe (E-mail: peggy.cebe@tufts.edu)

ABSTRACT: Poly(L-lactic acid) (PLLA)-aligned fibers with diameters in the nano- to micrometer size scale are successfully prepared using the electrospinning technique from two types of solutions, different material parameters and working conditions. The fiber quality is evaluated using scanning electron microscopy (SEM) to judge fiber diameter, diameter uniformity, orientation, and appearance of defects or beads. The smoothest fibers, most uniform in diameter and defect free, were found to be produced from 10% w/v chloroform/dimethylformamide solution using an accelerating voltage from 10–20 kV. Addition of 1.0% multiwalled carbon nanotubes (MWCNT) into the electrospinning solution decreases fiber diameter, improves diameter uniformity, and slightly increases molecular chain alignment. The fibers were cold crystallized at 120°C and compared with their as-spun counterparts. The influences of the crystalline phase and/or MWCNT addition were examined using fiber shrinkage, temperature-modulated calorimetry, X-ray diffraction, and dynamic mechanical analysis. Crystallization increases the glass transition temperature, T_g, slightly, but decreases the overall fiber alignment through shrinkage-induced buckling of the fibers when heated above T_g. MWCNT addition has little impact on T_g, but significantly increases the orientation of crystallites. MWCNT addition slightly reduces the dynamic modulus, whereas crystallization increases the modulus in both neat- and MWCNT-containing fibers. © 2014 Wiley Periodicals, Inc. J. Appl. Polym. Sci. **2015**, *132*, 41779.

INTRODUCTION

Within the last two decades, electrospinning has become recognized as a highly versatile method to produce submicro and nanosized polymer fibers.[1–3] The fiber preparation occurs when a small diameter stream is drawn from a stock solution by an electrical force. Dry solid fibers will form after solvent evaporates from the stream.[4,5] The produced polymer fibers have been used as drug delivery carriers,[6] wound dressing,[7] in protective clothing,[8] and as chemical sensors.[9,10] Recently, electrospun polymer fibers have been proposed for new applications in conjunction with biomedical research in which they can be used as scaffolds for neural tissue engineering[11] and bioabsorbable membranes.[12] Biodegradable polymers have played a major role in biomedical applications, as these polymers are harmless to the environment and could have potential application within the human body. The objective of introducing polymer fibers as candidates for medical applications, such as simulating the directional growth of neurons, is that they can more precisely mimic a repair process that should be performed by the human body. The advantage of using electrospinning is attributed to the fact that fiber diameter and alignment can be controlled by the following: (1) material conditions, such as polymer molecular weight, and solution concentration, and polarity; and (2) working conditions, such as flow rate, needle to collector distance, voltage, humidity, and collector type. Positive results of growth of C17.2 cells on aligned poly(L-lactic acid), PLLA, electrospun nanofibrous scaffold were reported in the literature.[11]

PLLA is a crystallizable thermoplastic polyester that is both biodegradable and biocompatible.[13–15] PLLA is the left-handed optical isomer of poly(lactic acid), PLA. It is made from renewable resources, such as corn or sugar cane. PLLA can be blended,[16,17] copolymerized,[7,13] or made into composites by addition of fillers[18–24] to improve its properties. Its glass transition temperature, T_g, is about 55–60°C,[25] and its melting temperature is about 150°C. Crystallization occurs by cooling from the melt or by heating the glass above T_g,[26–28] though crystallization from the

melt can be slow enough that amorphous samples are readily obtained by fast cooling.[29] The slow crystallization of PLLA has the impact that fibers prepared from solution during electrospinning can solidify without crystallization.[16] In this study, we demonstrate the successful production of PLLA fibers with high alignment and smoothness, with the fiber morphological quality evaluated using scanning electron microscopy (SEM). The effects of existence of crystalline phase and/or addition of multiwalled carbon nanotubes (MWCNTs) are evaluated for their impact on fiber structure (diameter, orientation, and elastic shrinkage),[30–35] on thermal properties, using modulated differential scanning calorimetry (MDSC), and for mechanical reinforcement by dynamic mechanical analysis (DMA). It is known that addition of MWCNTs into electrospun fibers changes the fiber dielectric constant[36] and conductivity[37] which could be important for controlling the fiber's diameter[38] and for the use of electrical triggers to stimulate cell growth when the fibers are used as supporting scaffolds.

The crystal formation and orientation are studied using X-ray diffraction showing development of crystal diffraction peaks, which have been studied previously and indentified as PLLA α-phase crystals.[39–43] The results of this study will present us with more detailed properties of aligned PLLA electrospun fibers with and without carbon nanotubes and give guidelines for picking suitable fibers for potential use in guiding growth of neurons or other cell types and for biomaterial applications. The results obtained are expected to help our understanding of the relationship between the structure and properties of polymer composites reinforced with nanoparticles. In particular, here, we show that PLLA fiber diameter and diameter distribution, fiber alignment, crystallite alignment, fiber shrinkage, and thermal properties can be quantified and related to the inclusion of MWCNTs into the electrospinning solution.

EXPERIMENTAL

Materials

Poly(L-lactide acid) 3051D was purchased from NatureWorks and used as received in pellet form. The pellets show white color, indicating existence of crystals, which is also specified by the manufacturer's online document.[44] To prepare polymer solutions for electrospinning, we tested two types of solvent. Hexafluoroisopropanol (HFIP) was obtained from Oakwood Chemical, and was used as the first solvent. Solutions with 5, 10, and 15 w/v % concentration were prepared after stirring for 24 h at room temperature to dissolve as much polymer as possible before electrospinning. All solutions prepared using HFIP were cloudy, and the solution did not clarify even after several days of stirring. Increasing the temperature of the stirred solution did not reduce the turbidity. This suggests HFIP is incapable of completely dissolving the crystals in the PLLA pellets. This problem is solved by introducing the second solvent system: chloroform and dimethylformamide (DMF). Both of them were obtained from Aldrich and used in a 3:1 v/v ratio and both 10 and 15 w/v % solutions were prepared. For this second-type solvent (which we will refer to as C/D), we dissolved PLLA in chloroform first with overnight stirring and then added DMF to reach the desired volume. All polymers in C/D solvent mixtures were stirred overnight at room temperature

to create uniform transparent solutions. In order to show the comparison between PLLA fibers with or without MWCNTs, another set of solutions and electrospun fibers were made using the exact same solution concentration as the second-type samples (in chloroform/DMF 3:1 v/v) but with 1.0% by weight of MWCNT added (referenced to the polymer weight). For polymer solutions with 1.0% MWCNT, 15 minutes of ultrasonication was conducted to separate CNTs from their bundles and disperse them evenly before electrospinning.

Electrospinning Process

A glass syringe (inner diameter 14.6 mm) with an 18 gauge stainless steel needle was locked onto a syringe pump (Braintree Scientific, Inc. BS-8000), loaded with about 5 ml of solution. A fixed feeding rate of 2 mL/h was set for all electrospun samples in this study. A rotating drum, covered by grounded copper conductive tape, is used to collect fibers with default rotating speed of 2000 rpm. A high-voltage power supply (Gamma High Voltage Research Inc. Model No. ES30P-5w) is used to charge the solution, providing applied voltage of 10 to 25 kV for this study. Aligned fibers were created successfully at room temperature for most electrospinning working conditions (with some exceptions mentioned in the Results and Discussion section). Our electrospinning chamber is an open one and operates at the relative humidity of the laboratory. We are not able to control humidity separately, though this variable is known to affect electrospinning results.[45,46] The as-spun fibers are peeled off from the rotating drum collector and dried of residual solvent by keeping in a vacuum oven at room temperature for 24 h before use. To prepare crystallized fiber mats for further testing, samples were held at 120°C in a Mettler hot stage for 1 h to crystallize the PLLA.

Scanning Electron Microscopy

SEM imaging is conducted using a Phenom Pure SEM at Tufts University. PLLA electrospun fiber samples were adhered onto the sample holder with double-sided carbon-conductive tape and precoated with gold using a sputter coater (Cressington Scientific sputter coater 108) for 40 s at 20 mA within an 0.8 psi argon gas environment, which add a dark gray-colored layer onto the fiber surface. During the SEM imaging, the voltage for SEM was 5 kV, while proper magnifications (2000 to 10,000) are used to insure we could measure the fiber diameter easily for both as-spun and crystallized samples. To ensure the accuracy of the statistical value of the fiber diameter, seven to 10 images were taken from different locations on each sample to obtain a reasonable estimation of the average fiber diameter.

Fiber orientation distribution was determined from analysis of SEM images of amorphous fibers with ImageJ using the plug-in application, OrientationJ. Two to three images were examined for each fiber type. If fibers were perfectly aligned with one another, they would be parallel along the circumference of the collector wheel and would lie perpendicular to the angular velocity of the wheel. OrientationJ allows us to evaluate the degree of misalignment of imperfectly deposited fibers.

Molecular Retraction

Polymer chains in electrospun fibers have been stretched by the electrical force when fibers are traveling from the needle tip to the collector and further stretched by the mechanical force of
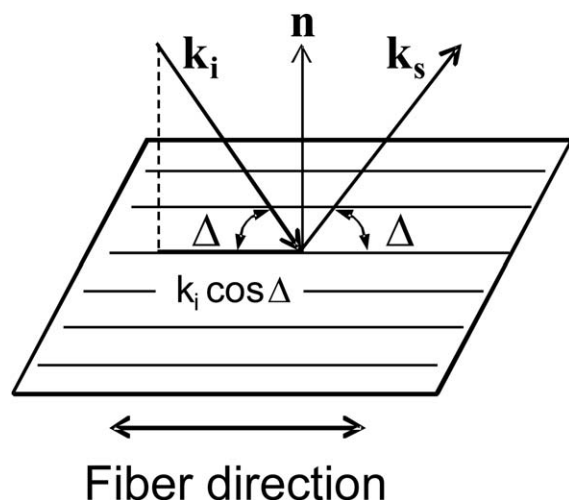
Figure 1. Sketch of mounting the fiber mat sample into the X-ray diffractometer, showing the incident and scattered *k*-vectors (k_i, k_s), sample normal (*n*), and fiber alignment direction. The projection $k_i \cos\Delta$ is parallel to the fiber direction, and *n*, k_i, k_s are coplanar.

the rotating drum electrode.[19] These partially aligned chains can show significantly different phenomenon such as polymer chain confinement and aligned lamella crystal formation. However, although it can be easily indentified, the alignment is hard to compare among different fibers. The method that we used is an indirect measurement. We use fiber elastic shrinkage ratio to investigate the polymer chain relaxation mechanism. The test is performed using an oil bath to heat samples to 160°C by submerging them in silicon oil. The length and width reductions are obtained using a digital caliper to measure sample dimensions before and after heat treatment. Four samples of each preparation were tested.

Wide-Angle X-ray Scattering (WAXS)
One-dimensional X-ray diffraction was performed in reflection mode (Figure 1) using a Philips PW 1830 powder diffractometer. The generator produced X-rays of wavelength $\lambda = 0.1542$nm (Copper K_α radiation) and was operated at 40 kV and 45 mA. Samples were examined in $\theta/2\theta$ reflection mode (for θ the half scattering angle) using a step scan interval of $0.02°$/step and scanning rate of $0.01°$/s from $2\theta = 5° - 35°$. A piece of ES fiber mat was cut and attached to a rectangular sample holder. The samples were positioned so that the incident and diffracted *k*-vectors k_i, k_s, and the sample normal, *n*, were coplanar. The projections into the plane of the sample mat, $k_i \cos\Delta$ *and* $k_s \cos\Delta$, were parallel to the fiber direction, as shown for the incident beam in Figure 1.

Collection of two-dimensional diffracted intensity was performed in transmission mode at the Brookhaven National Synchrotron Light Source, beam line X27C. Fibers were mounted with fiber direction perpendicular to k_i. Wavelength was 0.1371 nm, and the sample-to-detector distance was 15.94 cm, calibrated with Al_2O_3 reference powder. Intensity was collected for 30 s with a MAR CCD detector and corrected for air background. To estimate the crystallite orientation, an annular

region centered on the origin of reciprocal space was selected, which contained the most intense 110/200 arc-like reflection of PLLA crystals.[39–43] WAXS intensity was first integrated along the radius direction (width) of the annulus, and then, the intensity variation around the annulus was analyzed. The full width at half maximum of the 110/200 arc allowed a rough estimate of the crystallite orientation for comparison of differently treated fiber samples.

Differential Scanning Calorimetry (DSC)
Thermal analysis is carried out using a TA Instruments Q100 temperature modulated DSC (MDSC), which was calibrated using indium and sapphire standards and used with 50 mL/min nitrogen gas flow in the chamber. The mass difference of sample and reference lid/pan was controlled within 0.03 mg. The samples were made from folded electrospun fiber mat, which was then confined between an aluminum pan and lid with mild pressure, therefore allowing free fiber shrinkage.[19] Samples were heated from room temperature to 70°C to relax the fiber above T_g ($T_g \approx 60°C$). Then, the samples were cooled to 30°C and heated to 180°C. During heating from 30°C, a rate of 5°C/min was used, with temperature oscillation amplitude of 0.796°C and period of 60 s.

Dynamic Mechanical Analysis (DMA)
TA Instruments RSA III was employed to perform dynamic mechanical analysis for both as-spun and crystallized fibers. Fiber mat was attached to a rectangular "picture frame" cardboard (which has a rectangular hole in the middle) and the two ends fixed using Kapton™ high-temperature tape. The cardboard frame helped the mounting of the fiber mat onto the tensile grips of the transducers, with direction of the fiber mat vertical and parallel to the direction of applied stress, and the frame was cut before testing. Samples were heated from 30°C to 100°C with a 3°C increment and tested under 0.1, 1, 10, and 50 Hz oscillation frequency.

RESULTS AND DISCUSSION

Fiber Morphology
SEM imaging of electrospun fibers gives us evidence to evaluate fiber quality, judging by the fiber alignment, diameter and diameter uniformity, surface smoothness, and the presence of defects or beads. The results of the fibers produced from HFIP 10% and 15% solutions are surprisingly good. Even with some of the undissolvable crystalline polymer remaining in the turbid solution, electrospun fibers still show smooth surfaces without any noticeable fracture, and only a few beads can be observed in the as-spun fiber. Electrospun fibers from 10% HFIP solution spun using different high voltages are shown in Figure 2(a–c). Compared to PLLA fibers used in a previous study for neuron growth,[11] the appearance of ES fibers from HFIP are already qualified as nanoscaffolds for neuron growth. In contrast to the 10% HFIP solution, the 5% HFIP solutions can hardly be electrospun into fibers at any of the voltages used. Fibers from 5% HFIP solution had many beads, showing the solution is too dilute to produce good fibers.[47] Despite the use of HFIP which is volatile and evaporates at low temperature (about 60°C), we did not observe pore formation on the fiber surface, such as that observed by Bognitski *et al.*[48]
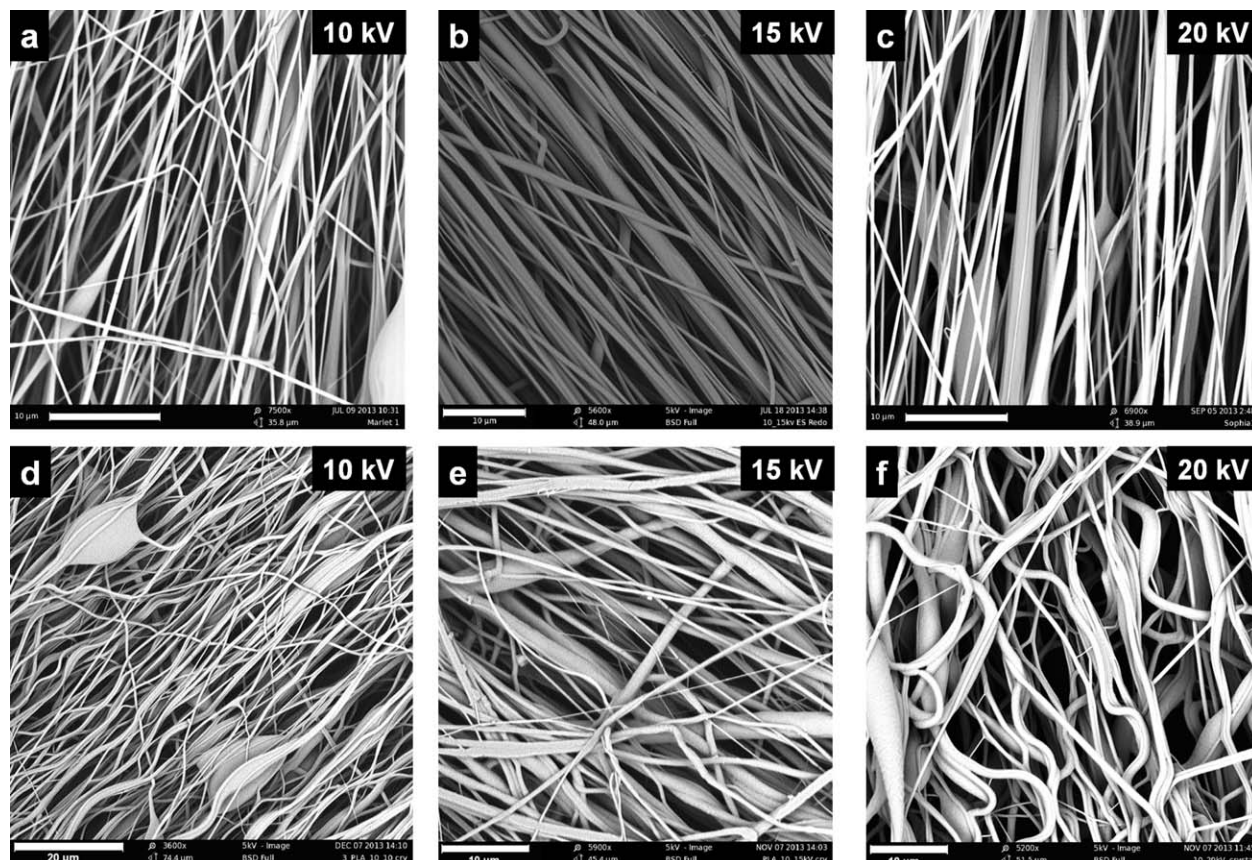
Figure 2. SEM images of PLLA fibers from 10% HFIP solution using 10, 15, or 20 kV as indicated. (a–c) as-spun amorphous fibers; (d–f) fibers crystallized at 120°C for 1 h. Scale bar is 20 μm in part (d), and 10 μm in all other figure parts.

It is well known that the crystal fraction of polymer has significant impact on polymer properties. Our heat treatment involves the isothermal crystallization of as-spun fiber at a temperature of 120°C for 1 h. Changes of fibers are observed using SEM as they no longer retain their original morphology: stretched aligned fibers become curved due to molecular retraction; more clumps are formed by several neighboring fibers sticking together [Figure 2(d–f)]. This part of the experiment shows the overall trend, leading to fiber deformation that occurs when temperature increase above T_g, which allows the polymer chains to retract freely. After molecular retraction and crystallization, curved fibers with more thick fibers and formation of beads or spindles are shown to occur. Curved fibers and gigantic beads or spindles are clear indication of improper surface environment for directed neuron growth.

The problem that HFIP could not fully dissolve the crystallized PLLA pellets is solved using the second type of solvent that is the mixture of chloroform/DMF in 3:1 volume ratio. In C/D solutions prepared with 10 and 15 w/v % PLLA, crystals have been dissolved as supported by the evidence of clear transparent solutions. Similar to the 5% HFIP solution, we found 5% C/D solution proved too dilute and difficult for electrospinning. The 15% solution is too thick, yielding only micron-sized fibers. With electrospun fibers from 10% solution, the best among them is the fiber prepared using 10–20 kV. SEM images are shown in Figure 3(a–d) along with the histograms [Figure

3(e–h)] showing the fiber diameter distribution. SEM images of crystallized PLLA fibers from C/D solvent (images not shown) had trends similar to fibers from HFIP solvent. Crystallization caused fibers to stick together, lose orientation, and buckle because of shrinkage during heating above the glass transition temperature (T_g).

A clear improvement is found for all fibers produced when 1.0% MWCNTs are added into the ES solution (Figure 4). The smoothness of the ES fiber surface indicates the MWCNTs only exist inside the fiber and presumably will not be toxic to living cells grown on the fiber surface. While the MWCNTs cannot be observed inside the fibers (transmission electron microscopy (TEM) would be needed for direct observation[49]), previously, we demonstrated their existence using ultracentrifugation to collect the MWCNTs from fibers after dissolution.[50] The line histogram of the as-spun fibers (Figure 4d) shows thinner fibers and narrower diameter distribution with added MWCNTs. Most fibers with 1.0% MWCNTs show diameters from 0.6 to 1.2 μm, which could be another effective controllable parameter for smaller diameter fiber preparation, in addition to the method found by Zong et al.[12] who used ionic salts in the ES solution for diameter control. From Figure 4(a–c), we observe that there is a general tendency for the fibers containing MWCNTs to be less well oriented. We surmise that the thinner, and hence lighter, fibers may undergo more whipping action in the Taylor cone region, and land on the collector wheel in a more
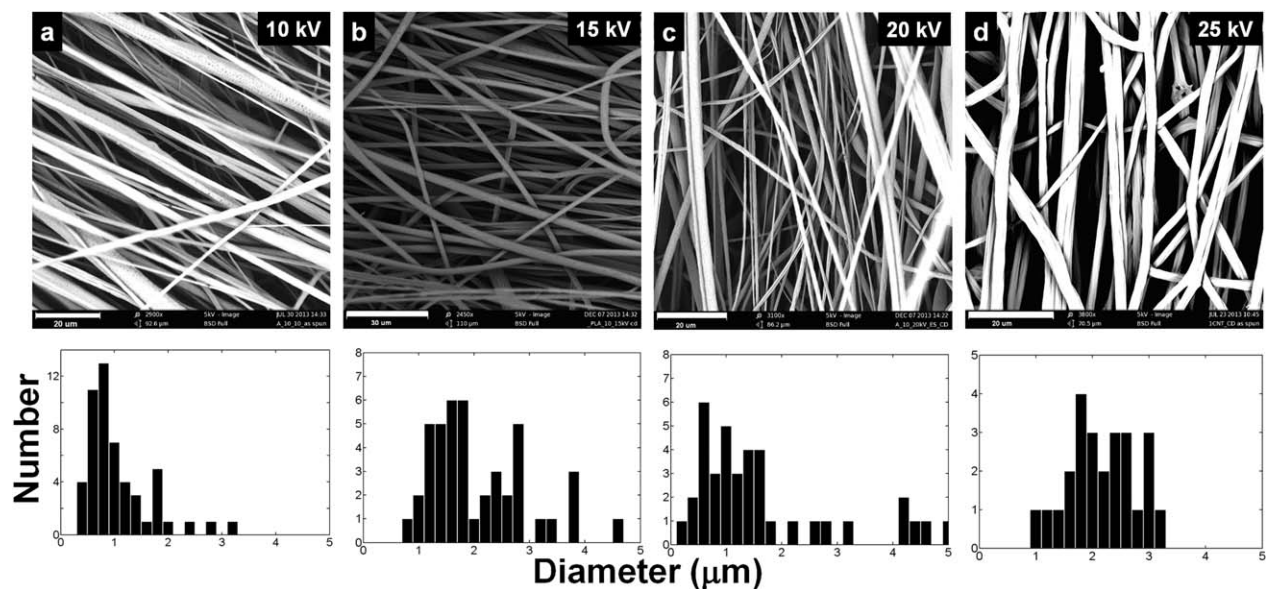
Figure 3. SEM results of as-spun PLLA fibers from chloroform/DMF solution 10% (a–c), or 15% (d), using different electrospinning voltages of 10, 15, 20, or 25 kV, as indicated. Scale bar is 30 μm in (b) and 20 μm in all other figure parts. The 15% solution shows high viscosity, yielding micron-sized fibers which could only be obtained after increasing the voltage to 25 kV (d). Histograms of each ES fiber type are shown below in e–h.
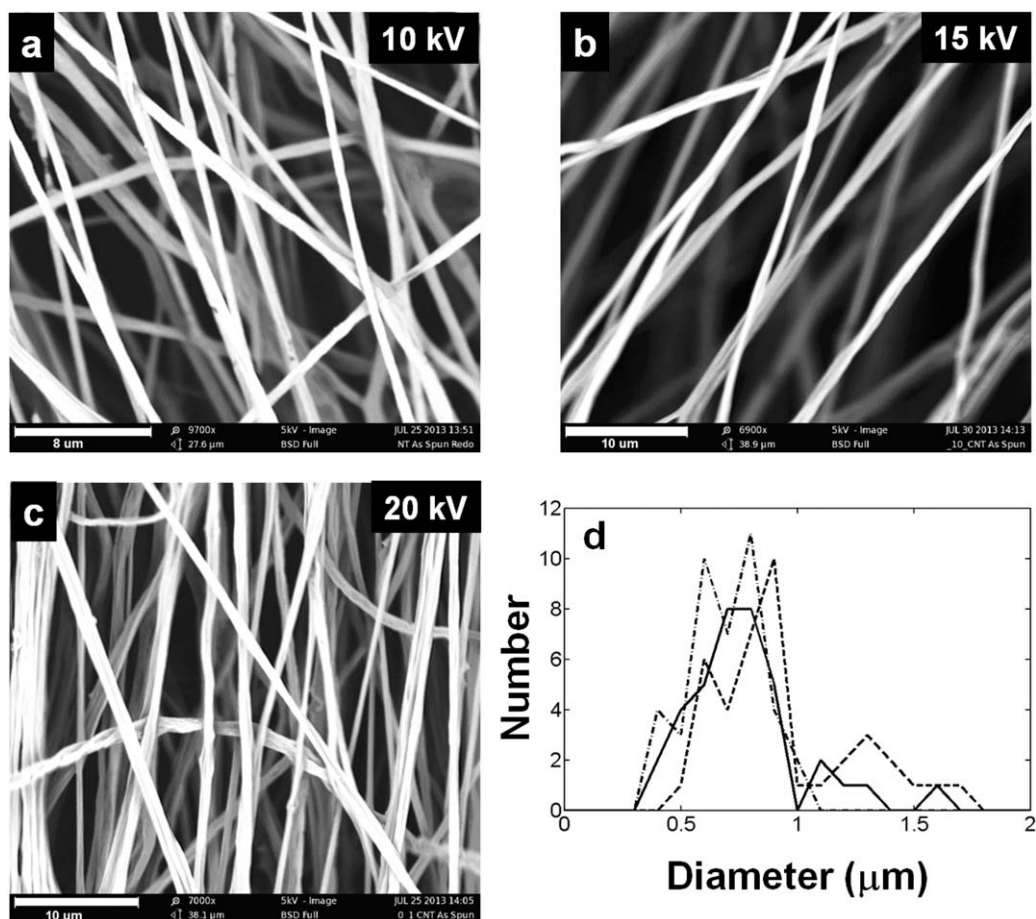

Figure 4. PLLA fibers from 10% C/D solution with 1.0% MWCNTs. (a–c): SEM images using: 10, 15, or 20 kV, as indicated. Scale bars are 8, 10, and 10 μm, respectively. (d) Line histogram enabling comparison of fibers prepared using accelerating voltage of 10 kV (solid), 15 kV (dashed), or 20 kV (dot dashed).
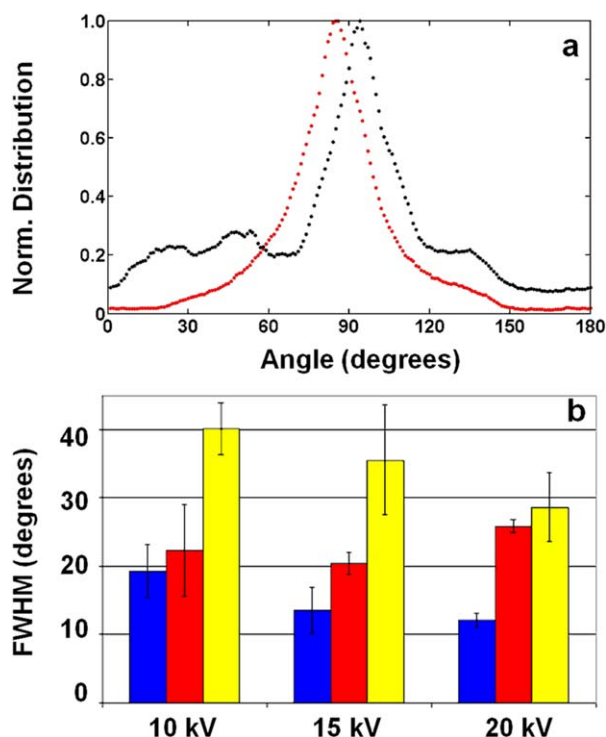
Figure 5. (a) Normalized orientation distribution versus angle from SEM images of amorphous PLLA fibers determined from OrientationJ. Fibers are from 10% C/D solution spun at 20 kV: neat PLLA (red), with 1% MWCNT (black). The angles are referenced to the vertical of the SEM image (set to 90°) and normalized to the maximum of the distribution. (b) The full width at half maximum of fiber distributions for HFIP (blue), C/D neat (red), C/D with 1% CNT (yellow), 10% solutions, at the indicated voltages. Error bars reflect the standard deviations. [Color figure can be viewed in the online issue, which is available at wileyonlinelibrary.com.]

disorganized manner. Fiber orientation is quantitatively assessed in the following section.

Fiber Orientation and Shrinkage
During spinning, the fibers land on the rotating collector wheel, and if they were perfectly aligned with one another, the long fiber axis would lie circumferentially on the wheel and perpendicular to the angular velocity of the wheel. However, due to instability of the fibers in flight, they may land in a somewhat disorganized manner on the wheel, which can be appreciated from the images in Figures 2–4. Average fiber orientation (alignment) was determined from analysis of the SEM images of amorphous fibers. OrientationJ software allows the distribution of the fiber orientation angles to be analyzed with respect to the image vertical direction and then presented as an angular distribution function, such as that shown in Figure 5a for fibers from 10% C/D solution spun at 20 kV. In the normalized distribution, neat fibers (red) have a single peak in the distribution of fiber orientation angles, whereas fibers containing MWCNTs (black) show (by the smaller secondary maxima) that there are some fibers misaligned at other angles. Figure 5b shows a plot of the full width at half maximum (FWHM) of the angular spread of the major peak in the fiber orientation distribution

function, for 10% solutions of neat PLLA fibers from HFIP or C/D solvent, and PLLA fibers containing 1% MWCNT as a function of the accelerating voltage.

The greater the FWHM in Figure 5, the less well oriented are the fibers. PLLA fibers from HFIP (blue) are the best oriented fibers, with FWHM always below 20°. As voltage increases, the fibers from HFIP solvent become more oriented. Neat PLLA fibers from C/D solvent are better oriented than their MWCNT-containing counterparts at 10 kV or 15 kV. The MWCNT-containing PLLA fibers had poor orientation at low accelerating voltages. It is likely that these thinner fibers experienced more chaotic motion during flight and landed on the collector wheel in a more disordered manner. As with the PLLA neat fibers from HFIP, the fibers containing MWCNTs had improvement in orientation as voltage increased.

As a direct phenomenon showing molecular retraction, fiber shrinkage occurs when samples are heated above T_g as polymer chains gain conformational mobility. We have used this approach in the past to characterize isotropic electrospun mats collected onto a static plate,[50] rather than the rotating drum used here. In that work, on PET electrospun with and without MWCNTs, we showed that mats containing MWCNTs underwent greater retraction, suggesting that the presence of MWCNT caused a greater initial molecular chain alignment during electrospinning.[50] We apply the same approach here to ES fibers collected on the rotating drum, which causes overall orientation of molecular chains along the direction of the fiber axis (tangent to the drum). The amount of reduction in fiber length or width shows the polymer chain's elastic relaxation from stretching by the electrical and mechanical forces, reflecting the internal stress level for as-spun fibers. The elastic shrinkage, S_e, is calculated as follows:

$$S_e = (1 - (\text{Final dimension}/\text{Initial dimension})) \times 100\%$$

Results of the molecular retraction test are shown in Figure 6 where width and length shrinkage of the fiber tapes are compared. Width shrinkage ranges from about 15% to 38%, which is less than the length shrinkage that ranges from about 49% to 60%. Shrinkage of fiber tapes prepared from HFIP was somewhat erratic most likely due to the presence of beads. We presume that the polymer molecules within the beads are less well oriented than those within the fibers. Comparing among the fibers prepared from C/D solution, fibers containing carbon nanotubes have greater width and length shrinkage than neat fibers. Surprisingly, an increase in the accelerating voltage did not result in an increase in the elastic shrinkage. If anything, a slight decrease in shrinkage was observed at 20 kV compared to 10 kV and 15 kV. This could indicate that the larger accelerating voltage causes more chain disentanglement during the fiber flight, which resulted in smaller elastic retraction.

Fiber Crystal Orientation
Crystal fraction is an important factor that will influence polymer thermal and mechanical properties. The crystal formation during isothermal crystallization is confirmed using one dimensional X-ray diffraction (Figure 7). Compared to as-spun fibers, crystallized PLLA fibers clearly show four diffraction peaks,
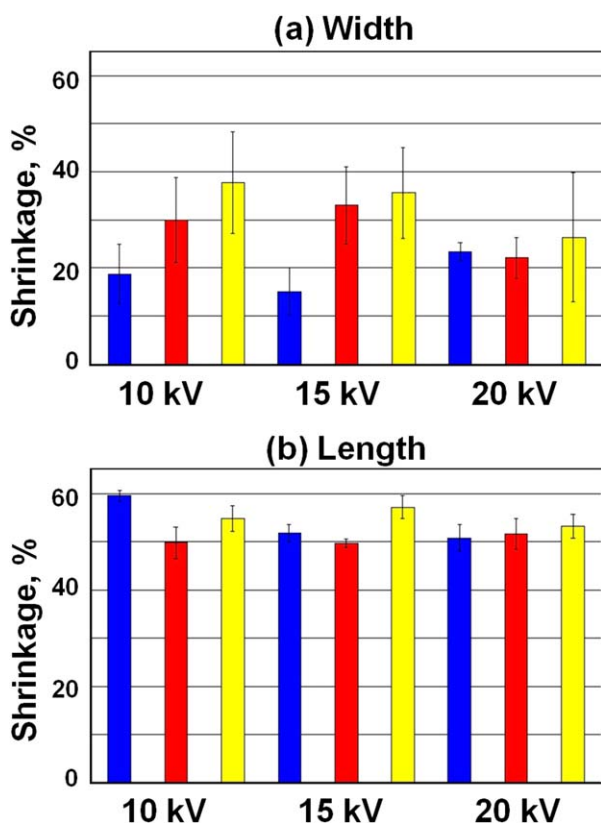
(a) Width

(b) Length

Figure 6. Shrinkage of ES fiber width (a) and length (b). Neat fibers prepared from HFIP (blue). Fibers prepared from C/D: Neat (red) or containing 1.0% MWCNTs (yellow). The same three fiber types are shown as a function of accelerating voltages: 10 kV, 15 kV, or 20 kV. Three samples of each type were tested, and error bars reflect the standard deviations. [Color figure can be viewed in the online issue, which is available at wileyonlinelibrary.com.]

which is evidence of crystal formation, resulting in the formation of α crystals.[39–43]

Two-dimensional images are presented in Figure 8(a,b), for neat, crystalline PLLA fibers prepared from 10% solution concentration, using accelerating voltage of 15 kV, but prepared from either HFIP (Figure 8a) or chloroform/DMF (Figure 8b) solvent. Crystals prepared from HFIP are more ordered than those from chloroform/DMF, as shown from the narrower spread of the 110/200 intensity arc in panel (a). The normalized intensity (i.e., normalized to a maximum of unity and minimum of zero) around 180° of the azimuth is presented in Figure 8c, for neat PLLA (blue) and for PLLA containing 1% of MWCNT (red), showing that improved orientation of crystallites (narrowing of peak intensity) is brought about by the addition of carbon nanotubes.

Figure 8d compares the full width at half maximum of the normalized semiazimuthal intensity for a variety of treatments. We can make the following general observations: Fibers prepared from HFIP solvent have better crystallite orientation at all voltages than fibers from CD solvent. PLLA fibers containing 1.0% of MWCNTs have better crystallite orientation than their neat counterparts, despite the occurrence of some beads in the sam-

ples from HFIP. Orientation improves (FWHM decreases) the most as voltage increases from 10 to 15 kV; only a modest improvement in orientation is brought by the change from 15 to 20 kV. Solutions made with C/D solvent have worse orientation at 15% solids content than at 10% solids. The 15% solutions were very viscous and could only be spun at 25 kV.

In all cases, the angular FWHM measured for the crystalline 110/200 peak is greater than the FWHM of the fiber orientation distribution function, which means the crystallites in disordered fibers are more misoriented on average than just the fibers. For example, for fibers containing 1% MWCNTs, the fiber orientation in Figure 5b ranges from about 28 to 40° (at 10 to 20 kV), whereas the crystallite orientation from Figure 8d varies from 44 to 52° over the same range of accelerating voltages. We cannot separately evaluate the crystallite orientation, since it is a function of the fiber orientation. However, this method does allow the qualitative comparison of fiber orientation and crystallite orientation among the various fiber preparations.

Fiber Thermal Properties and Crystallinity

Most cells are sensitive to temperature and can only survive within strictly controlled environment under physiological conditions of pH and temperature. However, for other applications of ES fibers, the higher temperature thermal properties are important factors for their application. Thermal behavior changes of as-spun PLLA ES fibers are shown in the MDSC heat flow rate versus temperature plot (Figure 9). In the total heat flow curve (dashed curves), the glass transition is interfered with by fiber shrinkage, a nonreversing event, shown by an endothermic peak as the polymer chains transit from a stretched state of lower entropy to one of higher entropy. Initially, amorphous fibers undergo cold crystallization at T_c followed by melting at T_m. Thermal data for T_g, T_c, and T_m are summarized in Table I. One change for the electrospun fiber, obtained from the reversing heat flow (solid curves), is that the glass transition temperature (T_g) increases 2–4°C for crystallized fiber compared to as-spun fiber. In addition, the table lists the area of the cold crystallization exotherm and melting endotherm
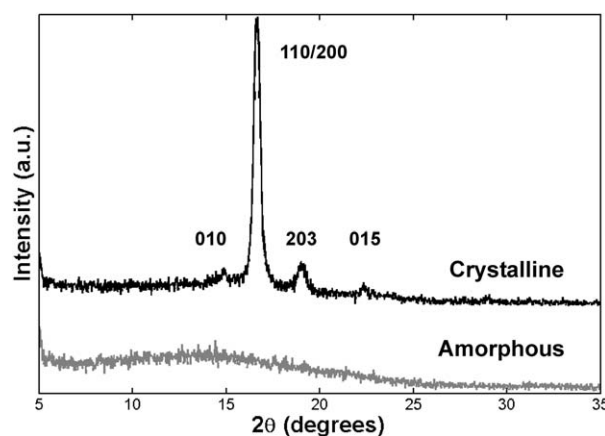

Figure 7. Typical 1D X-ray diffraction of neat PLLA ES fibers from 10% chloroform/DMF solution using 10 kV; as-spun amorphous fiber (gray) and the same sample after isothermal crystallization at 120°C for 1 h (black). The Miller indices are shown above the crystalline reflections.[39–43]
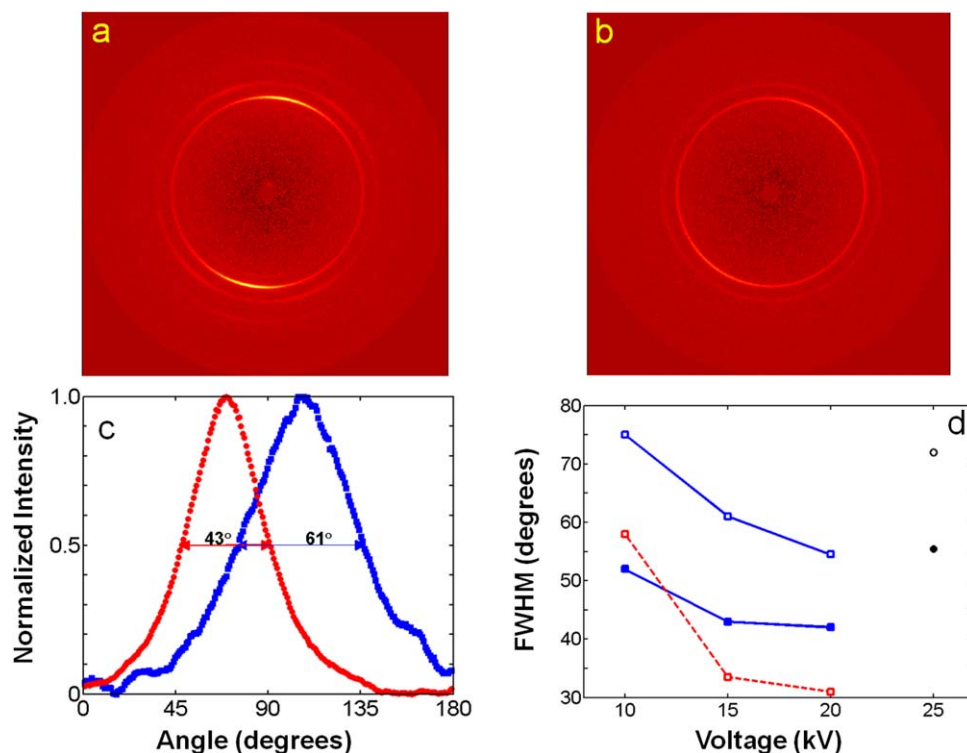
Figure 8. PLLA prepared from 10% solution at 15 kV and crystallized at 120°C for 1 h. Two-dimensional WAXS images of neat PLLA from: HFIP solution (a) or chloroform/DMF solution (b). (c) Comparison of normalized semicircumferential intensity versus relative azimuthal angle, for the sample shown in (b) (blue) and the same type of sample but containing 1% of MWCNT (red). The FWHM angular spread is indicated. (d) Comparison of the FWHM versus accelerating voltage, for neat PLLA (open symbols) or PLLA containing 1% of MWCNT (filled symbols). PLLA prepared from 10% (blue) or 15% (black) chloroform/DMF, or 10% HFIP (red). [Color figure can be viewed in the online issue, which is available at wileyonlinelibrary.com.]

determined from the total heat flow rate scan. The area of the crystallization exotherm is always less than that of the corresponding endotherm, even after correction of the heat of fusion for degree of undercooling by the factor, f,[51] using the relationship $f = 2T/(T + T_m^0)$. The small variation between ΔH_f and ΔH_c results in an assumption that the degree of crystallinity might not be zero at the start of the scan for as-spun samples. The apparent degree of crystallinity, ϕ_c, is shown in the last column of Table I, and for as-spun fibers ranges from 0.01–0.05. However, no crystallinity was observed in X-ray diffraction for the as-spun samples. This disparity may possibly result from inability to determine clearly the start of the exotherm due to interference from the fiber shrinkage that occurs in the same temperature range. After crystallization at 120°C for 1 h, ϕ_c ranges from 0.30–0.35 and is unaffected by the presence of carbon nanotubes. In making the calculation of the degree of crystallinity, we use the heat of fusion from Pyda et al.[25] 91 J/g, rather than the slightly larger value reported earlier by Fischer et al.[52] Unlike Pan et al.,[28] we did not observe any multiple melting behavior in the cold crystallized samples.

Interestingly, despite both theoretical and experimental approaches appearing in the literature suggesting a decrease in T_g,[20,24] judging by reversing the heat flow curves in Figure 9, the addition of 1% MWCNTs does not have a strong influence on T_g of as-spun PLLA fibers. Our result is consistent with that of Papageorgiou et al.[21] who also found MWCNT had no effect on the glass transition.

Mechanical Properties
Young's modulus data are presented to show the fiber modulus in the overall direction of alignment of the fibrous tape. Due to
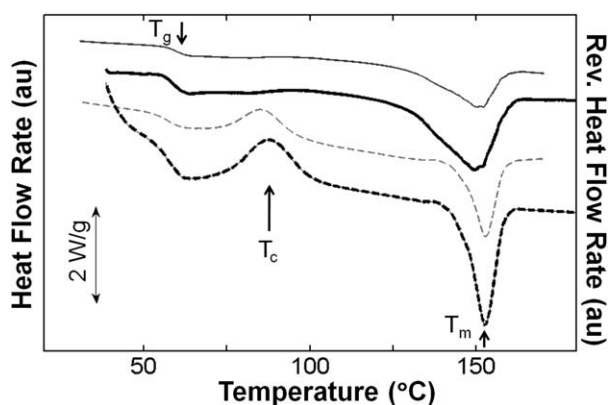

Figure 9. Typical MDSC scans showing the heat flow rate (dashed) and reversing heat flow rate (solid) of as-spun ES fibers prepared from a 10% chloroform/DMF solution using 10 kV, heated from 0°C to 180°C. Neat PLLA is depicted with heavy curves; PLLA with 1.0% carbon nanotubes is depicted with light curves. The glass transition, T_g, cold crystallization, T_c, and melting, T_m are marked. Curves have been displaced vertically for clarity.

Table I. Thermal Properties of Various PLLA Fibers[a] from DSC: Glass Transition, Crystallization and Melting Temperatures, Heats of Crystallization and Fusion, and Crystallinity

Voltage (kV)	PLLA[b]	$T_g \degree C \pm 0.5$	$T_c \degree C^c \pm 0.5$	ΔH_{c}, J/g ± 0.5	$\Delta H_c^{corr\,d}$ J/g ± 0.5	$T_m \degree C \pm 0.5$	ΔH_F J/g ± 0.5	$\phi_c{}^e \pm 0.02$
10	neat – as-spun	59.6	74.0	18.1	21.1	151.7	24.7	0.04
15	neat – as-spun	58.1	73.1	19.1	22.3	150.8	26.6	0.05
20	neat – as-spun	58.9	73.0	19.8	23.1	150.9	24.3	0.01
10	neat – crystal	61.8	–	0	0	153.1	27.6	0.30
15	neat – crystal	61.7	–	0	0	152.1	31.5	0.35
20	neat – crystal	61.1	–	0	0	153.6	28.6	0.31
10	1% CNT – as-spun	58.6	72.0	19.0	22.2	151.1	25.3	0.03
15	1% CNT – as-spun	59.4	73.2	18.4	21.5	152.0	26.4	0.05
20	1% CNT – as-spun	59.3	73.1	19.6	22.9	151.3	24.6	0.02
10	1% CNT – crystal	63.6	–	0	0	152.6	28.1	0.31
15	1% CNT – crystal	61.7	–	0	0	153.2	29.5	0.32
20	1% CNT – crystal	61.8	–	0	0	150.9	32.4	0.36

[a] Prepared from 10% solutions of chloroform/dimethylformamide.
[b] Prepared neat, or with 1.0% MWCNTs, either as-spun or crystallized for 1 h at 120°C.
[c] Peak temperature of the exotherm during nonisothermal heating.
[d] Heat of crystallization, corrected for degree of under cooling by $f = 0.86$ [51].
[e] Crystallinity at the start of the DSC scan found using $(\Delta H_F - \Delta H_c^{corr})/91$ J/g [25].

the limitation of conventional thickness measurement (which involves simply measuring the thickness of the fiber mat using a micrometer and will necessarily include the air gaps between fibers), a method is employed here to estimate the effective thickness of polymer alone, that is, effective thickness, d. First, we assume that the fiber mat has uniform thickness, t. The mass, m, of a rectangular mat is measured and used to calculate the total volume of the material $V = m/\rho_a$, where ρ_a is the known density of amorphous PLLA ($\rho_a = 1.248$ g/cm^3 [52]). Here, we neglect the difference between the amorphous and crystalline densities ($\rho_c = 1.283$ g/cm^3 [53]), contributing less than 3% error. The effective thickness is obtained as $d = V/(WL)$ where L and W are the length and width of the fiber mat, respectively. The meaning of the effective thickness, d, is that it is the thickness which the fiber mat would have, if all the air were removed, and length, L, and width, W, were the same, as
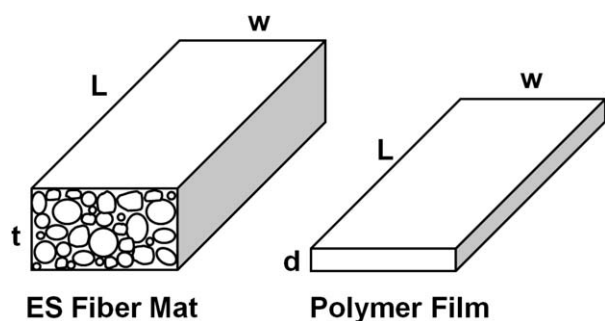

Figure 10. The cross-section sketch (left) shows an electrospun fiber mat, end on, with air gaps between fibers. The effective thickness, d, represents a polymer film (right) of the same length and width as the fiber mat, which has the same amount of polymer.

shown in Figure 10. Fiber consolidation and removal of air gaps when heating above T_g causes a decrease in thickness.

Dynamic mechanical data of storage modulus, E', and $tan(d) = E''/E'$ (where E$''$ is the loss modulus) of as-spun fibers (circle symbols) and crystallized fibers (square symbols) are shown in Figure 11(a,b), respectively. The cross-sectional area used in the modulus calculation is $A = W \times d$. The interpretation of DMA data for PLLA electrospun fibers shows several stages of Young's modulus change in Figure 11a when fibers are heated from 30°C to 100°C. At the beginning, $T < T_g$, the fibers are in the solid state giving a relatively higher modulus. When the temperature increases to the glass transition, the as-spun fibers (circle symbols) experience retraction. The shrinkage provides intense force on the DMA transducer giving a dramatic increase in the (apparent) modulus value. This point is supported by the absence of the intense peak during measurement of crystallized fiber (square symbols). After the shrinkage is completed, the temperature is higher than T_g, putting the fiber into the rubbery state, which is characterized by a decreased modulus compared to the glassy solid state. The system remained in this state until cold crystallization occurs when temperature increases above 70°C. The as-spun and crystallized fibers have the same value of rubbery modulus above 85°C, as both types are crystalline materials at this point. The $tan(\delta)$ data in Figure 11b show a strong peak caused by shrinkage in the as-spun fibers, and a smaller broad peak for the crystalline fibers. The glass transition assigned to the peak of $tan(\delta)$ is at a higher temperature for the crystalline fibers, which trend was also seen in the MDSC thermal data.

Several research groups have reported the Young's modulus of PLA. Garlotta[13] reports E' less than 3 GPa. Lin et al.[22] found that in melt-blended, compression-molded PLA containing up
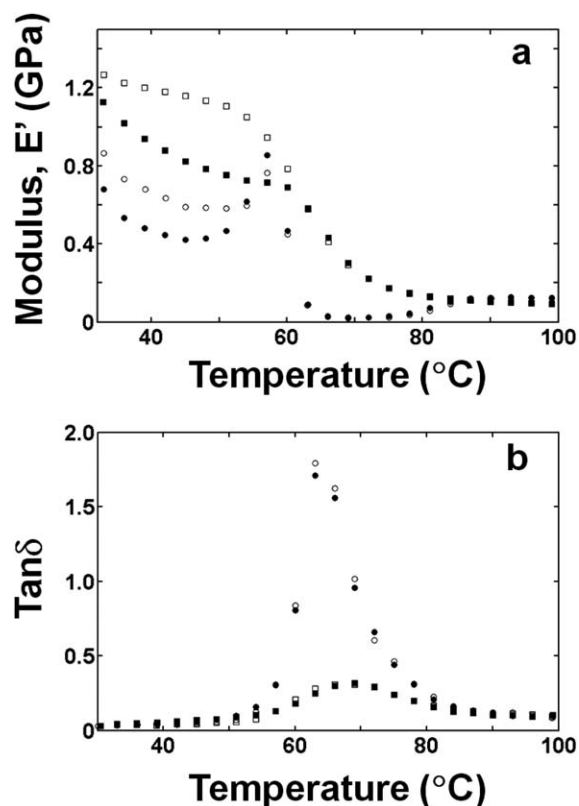
Figure 11. Mechanical properties of electrospun PLLA fibers from 10% C/D solutions, spun at 20 kV, and tested at 1 Hz. As-spun fibers (circles), crystalline fibers (squares), neat fibers (open symbols), fibers containing 1% MWCNT (filled symbols). Modulus (a) and Tanδ (b) versus temperature.

to 3 wt % of MWCNTs, the addition of nanotubes increased E′, giving values from 2–3 GPa. Papageorgiou et al.[21] used three-point bending tests and found a glassy modulus of 3 GPa for PLA/MWCNT composites. Picciochi et al.[55] reported on semicrystalline PLLA but only relative dynamic moduli were reported. In a review of PLLA properties, Gupta et al.[15] report that hot drawn fibers could have tensile moduli as high as 9.2 GPa, a result supported by theoretical calculations of Montes de Oca and Ward[56] for highly crystalline PLLA fibers in the direction transverse to the molecular chain. (Much higher crystalline modulus, E′ = 36 GPa, was predicted along the molecular chain direction.[56]) While the trends observed in our data agree with the prior literature, the glassy moduli measured are lower than the reported values. This could be a result of lack of interfiber entanglements in these nonwoven mats, causing poor stress transfer through the specimen.

Despite the common use of MWCNTs as a reinforcement nanofiller material reported in the literature and for commercial application,[54] in our study, the addition of MWCNT shows clear signs of weakening the fiber modulus in the fiber axis direction. There could be several possible reasons for this change. First, MWCNTs may have poor interaction with the PLLA polymer chains, also weakening the structure due to ineffective stress transfer. In this situation, the carbon nanotubes would act more

like a void, reducing the effective cross-sectional area of the sample for stress transfer. Second, adding MWCNTs into the solution yields fibers with diameter between about 0.6 and 1.2 μm, but fibers with larger or smaller diameters are missing, which may be bigger contributors to overall strength. Aggregation of MWCNTs in the electrospinning solution has been not taken into consideration, and the ultrasonication method has not been not quantitatively evaluated for efficiency, possibly leaving unseparated nanotubes bundles or breakage of the carbon nanotubes. Finally, the addition of MWCNTs may result in more fiber disentanglement, causing weaker stress transfer compared to the neat fibers.

We need to reiterate that the electrospun fibers undergo substantial shrinkage during testing and may have significant errors associated with the cross-sectional area determination as temperature increases. While the trends in the modulus are similar across the various fiber preparations, still the DMA data should be considered as qualitative with regard to the numerical values of the moduli. However, the general trend of lower elastic modulus in fibers containing MWCNTs has been verified by measurement of the elastic moduli of single PLA fibers using atomic force microscopy, in collaboration with the group of Prof. C. Staii and coworkers at Tufts.[36]

CONCLUSIONS

Aligned PLLA ES fibers are successfully prepared using electrospinning from both HFIP and chloroform/DMF solution. Although HFIP could not completely dissolve the crystal from PLLA pellets, fiber quality is promising, with smooth surface, good alignment, and few beads. The best ES parameters for PLLA from chloroform/DMF solution are found using 10 w/v % solution, and electrospinning at 10 kV, while holding constant the 12-cm needle to collector distance and rotating drum collector speed of 2000 rpm. We have used analytical techniques that are well known in polymer science to study electrospun fibers. These include assessment of the molecular retraction, fiber orientation, and crystallite orientation. Addition of carbon nanotubes results in reduced fiber diameter, and narrower diameter distribution, slightly reduced dynamic modulus, and larger fiber misalignment. The latter is possibly due to the lighter weight of the thinner MWCNT-containing fibers that land more chaotically on the collector wheel. Despite the larger fiber misalignment, MWCNT-containing fibers have a narrower crystallite orientation distribution than their neat counterparts at all accelerating voltages. Cold crystallization of neat and MWCNT-containing fibers increased the glass transition and the dynamic modulus but contributed to increased fiber disorder after shrinkage. In future work, we suggest to cold crystallize the fibers with ends fixed to prevent or at least minimize this disorder. With the exception of the fibers spun from 15% solutions, all other as-spun fibers can be considered as suitable substrates for biomedical applications.

REFERENCES

1. Doshi, J.; Reneker, D. H. *J. Electrostat.* **1995**, *35*, 151.

2. MacDiarmid, A. G.; Jones, W. E.; Norris, I. D.; Gao, J.; Johnson, A. T.; Pinto, N. J.; Hone, J.; Han, B.; Ko, F. K.; Okuzaki, H.; Llaguno, M. *Synth. Met.* **2001**, *119*, 27.

3. Behler, K.; Havel, M.; Gogotsi, Y. *Polymer* **2007**, *48*, 6617.

4. Huang, Z. M.; Zhang, Y. Z.; Kotaki, M.; Ramakrishna, S. *Compos. Sci. Technol.* **2003**, *63*, 2223.

5. Taylor, G. *Proc. R Soc. Lond. A Math. Phys. Sci.* **1969**, *313*, 453.

6. Zeng, J.; Xu, X.; Chen, X.; Liang, Q.; Bian, X.; Yang, L.; Jing, X. *J. Control. Release* **2003**, *92*, 227.

7. Toncheva, A.; Spasova, M.; Paneva, D.; Manolova, N.; Rashkov, I. *Int. J. Polym. Mater. Polym. Biomater.* **2014**, *63*, 657.

8. Gorji, M.; Jeddi, A. A. A.; Gharehaghaji, A. A. *J. Appl. Polym. Sci.* **2012**, *125*, 4135.

9. Thomas, S. W. III.; Joly, G. D.; Swager, T. M. *Chem. Rev.* **2007**, *107*, 1339.

10. Gerard, M.; Chaubey, A.; Malhotra, B. D. *Biosens. Bioelectron.* **2002**, *17*, 345.

11. Yang, F.; Murugan, R.; Wang, S.; Ramakrishna, S. *Biomaterials* **2005**, *26*, 2603.

12. Zong, X.; Kim, K.; Fang, D.; Ran, S.; Hsiao, BS.; Chu, B. *Polymer* **2002**, *43*, 4403.

13. Garlotta, D. *J. Polym. Environ.* **2001**, *9*, 63.

14. Nampoothiri, K. M.; Nair, N. R.; John, R. P. *Bioresour. Technol.* **2010**, *101*, 8493.

15. Gupta, B.; Revagade, N.; Hilborn, J. *Prog. Polym. Sci.* **2007**, *32*, 455.

16. Li, K.; Mao, B.; Cebe, P. *J. Therm. Anal. Calorim.* **2014**, *116*, 1351.

17. Di Lorenzo, M. L.; Rubino, P.; Cocca, M. *J. Appl. Polym. Sci.* **2014**, *131*, 40372.

18. Monticelli, O.; Bocchini, S.; Gardella, L.; Cavallo, D.; Cebe, P.; Germelli, G. *Eur. Polym. J.* **2013**, *49*, 2572.

19. Ma, Q.; Pyda, M.; Mao, B.; Cebe, P. *Polymer* **2013**, *54*, 2544.

20. Tsuji, H.; Kawashima, Y.; Takikawa, H.; Tanaka, S. *Polymer* **2007**, *48*, 4213.

21. Papageorgiou, G. Z.; Achilias, D. S.; Nanaki, S.; Beslikas, T.; Bikiaris, D. *Thermochim. Acta.* **2010**, *511*, 129.

22. Lin, W. Y.; Shih, Y. F.; Lee, C. H.; Lin, C. C.; Yu, Y. H. *J. Taiwan Inst. Chem. Eng.* **2013**, *44*, 489.

23. Mathew, A. P.; Oksman, K.; Sain, M. *J. Appl. Polym. Sci.* **2005**, *97*, 2014.

24. Li, Y.; Wu, H.; Wang, Y.; Liu, L.; Han, L.; Wu, J.; Xiang, F. *J. Polym. Sci. Part B: Polym. Phys.* **2010**, *48*, 520.

25. Pyda, M.; Bopp, R. C.; Wunderlich, B. *J. Chem. Thermodyn.* **2004**, *36*, 731.

26. Pan, P.; Kai, W.; Zhu, B.; Dong, T.; Inoue, Y. *Macromolecules* **2007**, *40*, 6898.

27. Kawai, T.; Rahman, N.; Matsuba, G.; Nishida, K.; Kanaya, T.; Nakano, M.; Okamoto, H.; Kawada, J.; Usuki, A.; Honma, N.; Nakajima, K.; Matsuda, M. *Macromolecules* **2007**, *40*, 9463.

28. Pan, P.; Zhu, B.; Kai, W.; Dong, T.; Inoue, Y. *Macromolecules* **2008**, *41*, 4296.

29. Chen, H. P.; Pyda, M.; Cebe, P. *Thermochim. Acta.* **2009**, *492*, 61.

30. Moniruzzaman, M.; Winey, K. I. *Macromolecules* **2006**, *39*, 5194.

31. Baughman, R.; Zakhidov, A.; de Heer, W. *Science* **2002**, *297*, 787.

32. Su, Z.; Li, J.; Li, Q.; Ni, T.; Wei, G. *Carbon* **2012**, *50*, 5605.

33. Ouyang, Z.; Li, J.; Wang, J.; Li, Q.; Ni, T.; Wei, G. *J. Mater. Chem. B* **2013**, *1*, 2415.

34. Xu, J.; Chen, T.; Yang, C.; Li, Z.; Mao, Y.; Hsiao, B. S. *Macromolecules* **2010**, *43*, 5000.

35. Ra, E.; An, K.; Kim, K.; Jeong, S.; Lee, Y. *Chem. Phys. Lett.* **2005**, *413*, 188.

36. Iqbal, Q.; Bernstein, P.; Zhu, Y.; Rahamim, J.; Cebe, P.; Staii, C. *Nanomaterials* **2014**, in review.

37. Jeong, J. S.; Jeon, S. Y.; Lee, T. Y.; Park, J. H.; Shin, J. H.; Alegaonkar, P. S.; Berdinsky, A. S.; Yoo, J. B. *Diamond Relat. Mater.* **2006**, *15*, 1839.

38. Baji, A. *Compos. Sci. Technol.* **2010**, *70*, 703.

39. De Santis, P.; Kovacs, A. *Biopolymers* **1968**, *6*, 299.

40. Alemán, C.; Lotz, B.; Puiggalí, J. *Macromolecules* **2001**, *34*, 4795.

41. Sasaki, S.; Asakura, T. *Macromolecules* **2003**, *36*, 8385.

42. Zhang, J.; Tashiro, K.; Domb, A. J.; Tsuji, H. *Macromol Symp.* **2006**, *242*, 274.

43. Di Lorenzo, M. L.; Rubino, P.; Luijkx, R.; Helou, M. *Colloid Polym. Sci.* **2014**, *292*, 399.

44. NatureWorks. NatureWorks PLA Polymer 3051D Injection Molding Process Guide. Minnetonka, MN: Natureworks LLC, **2006**.

45. Casper, C.; Stephens, J.; Tassi, N.; Chase, D.; Rabolt, J. *Macromolecules* **2004**, *37*, 573.

46. Cozza, E. S.; Monticelli, O.; Marsano, E.; Cebe, P. *Polym. Int.* **2013**, *62*, 41.

47. Lee, K.; Kim, H.; Bang, H.; Jung, Y.; Lee, S. *Polymer* **2003**, *44*, 4029.

48. Bognitski, M.; Czado, W.; Frese, T.; Schaper, A.; Hellwig, M.; Steinhart, M.; Greiner, A.; Wendorff, J. H. *Adv. Mater.* **2001**, *13*, 70.

49. Dror, Y.; Salalha, W.; Khalfin, R.; Cohen, Y.; Yarin, A.; Zussman, E. *Langmuir* **2003**, *19*, 7012.

50. Chen, H. P.; Liu, Z.; Cebe, P. *Polymer* **2009**, *50*, 872.

51. Hoffman, J. D.; Davis, G. T.; Lauritzen, J. I. In Treatise on Solid State Chemistry. Haney NB, Ed.; Plenum Press: New York, **1976**.

52. Fischer, E.; Sterzel, H.; Wegner, G. *Kolloid Z. Z. Polym.* **1973**, *251*, 980.

53. Hoogsteen, W.; Postema, A. R.; Pennings, A. J.; tenBrinke, G.; Zuganmaier, P. *Macromolecules* **1990**, *23*, 634.

54. Bokobza, L. *Polymer* **2007**, *48*, 4907.

55. Picciochi, R.; Wang, Y.; Alves, N. M.; Mano, J. F. *Colloid Polym. Sci.* **2007**, *285*, 575.

56. Montes de Oca, H.; Ward, I. *J. Polym. Sci. Part B: Polym. Phys.* **2007**, *45*, 892.